C Journal of Carbon Research

MDPI

Article

Morphological Characterization and Lumped Element Model of Graphene and Biochar Thick Films

Muhammad Yasir [1], Pietro Zaccagnini [2], Gianluca Palmara [2], Francesca Frascella [2], Niccolò Paccotti [2] and Patrizia Savi [1,*]

[1] Department of Electronics and Telecommunications, Politecnico di Torino, 10129 Torino, Italy; muhammad.yasir@polito.it
[2] Department of Applied Science, Politecnico di Torino, 10129 Torino, Italy; pietro.zaccagnini@polito.it (P.Z.); gianluca.palmara@polito.it (G.P.); francesca.frascella@polito.it (F.F.); niccolo.paccotti@polito.it (N.P.)
* Correspondence: patrizia.savi@polito.it

Abstract: Carbon based materials exhibit interesting mechanical, thermal and electrical properties which make them excellent contenders for use as fillers in composites as film. Graphene has been vastly used among the carbon-based materials. More recently eco-friendly carbon-based materials like biochar have emerged. The deployment of carbon-based materials in films needs to be studied since films are more versatile and permit the exploitation of electrical properties of such materials over circuits and systems. Typical circuits and systems exploiting electrical properties of novel materials perform a number of applications including sensing, detection, tunable devices and energy harvesting. In this paper, films composed of 9:1 graphene or biochar are deployed on a microstrip line. The morphological properties of graphene and biochar and their respective films are studied with Raman spectra and Field Emission Scanning Electron Microscope (FESEM). The electrical properties (four-point probe measurements and scattering parameter measurements) of the films. Low frequency measurements are used as starting point for circuit models estimating the lumped impedance of the films. From the morphological characterization it is shown that biochar films appear as granulates carbonaceous materials whereas graphene films contains several flakes forming a network. From the low frequency measurements and microwave characterization it is seen that graphene films are more conductive as compared to biochar films. In many applications, it is useful to know the surface impedance of the film since it varies on interaction with any external stimulus (variation of pressure, humidity, gas, etc.).

Keywords: graphene; biochar; thick films; microstrip lines; lumped model; scattering parameters

Citation: Yasir, M.; Zaccagnini, P.; Palmara, G.; Frascella, F.; Paccotti, N.; Savi, P. Morphological Characterization and Lumped Element Model of Graphene and Biochar Thick Films. *C* **2021**, *7*, 36. https://doi.org/10.3390/c7020036

Academic Editors: Craig E. Banks and Camélia Ghimbeu

Received: 31 January 2021
Accepted: 23 March 2021
Published: 27 March 2021

1. Introduction

There has been an increased interest in the use of carbon-based materials for a number of innovative applications due to their very attractive mechanical, thermal and electrical properties [1,2]. The most notable among the carbon-based materials is graphene, the electrical properties of which are exploited in a number of applications at microwave [3,4] and terahertz frequencies [5,6]. Graphene is a monolayer of carbon atoms attached to each other in the form a honeycomb crystal lattice. Graphene possess excellent thermal and electrical conductivity. It has a large surface area and is very light. Multi-layered graphene is used in films [7] and bulk composites [8,9] since large quantities are required instead of monolayer graphene. Multi-layered graphene in the form of nanocomposites can be easily produced therefore it is used as an alternative. The defects in graphitization grade is usually used to classify graphene based on its quality [10]. More recently biochar is another emerging carbon-based material due to it eco-friendly nature and low cost [11]. Biochar is obtained as a result of pyrolyzing organic wastes [12]. Since its synthesis does not require harsh solvents and other petroleum-based materials therefore it is considered ecologically friendly [13,14]. Furthermore, it has the capability to seize carbon from the environment

therefore it is considered carbon negative material, which is very useful given the fact that carbon emissions are ever increasing [15]. There is a variation in the electrical properties of biochar based on its origin however if compared to graphene, its electrical properties are inferior. There have been studies which found that the activation of biochar with a further heat treatment can make it more conductive [16,17].

In a number of applications where graphene and biochar are used in conjunction with electrical circuitry, they can only be deployed in the form of films. This makes it easy to manipulate them and use them in many applications [18–20]. In this form they can be modelled as lumped elements. The knowledge of the electrical properties of films in the form of lumped element model makes it possible to design systems for a number of applications. In fact, the conventional electrical readout circuits and systems are based on lumped elements theory.

In this work, we report a comparison between biochar and graphene nanoplatelet films. The two carbon materials and their films are morphologically investigated by Raman (level of defectiveness and graphitization) and Field Emission Scanning Electron Microscope (FESEM). Measurements are carried out at low frequency by four-point probe method in the frequency range 100 KHz–1 MHz. The films are deposited in a gap between two microstrip transmission lines. The scattering parameters (S_{11} and S_{12}) of the microstrip lines properly loaded with films are measured in the frequency band 1 GHz–5 GHz and the characteristics of the different films compared. A lumped element model is used to model the microstrip line gap and the deposited films. The values of lumped impedance are obtained by fitting the amplitude and phase of the simulated scattering parameters to the measured scattering parameters.

2. Materials and Methods

2.1. Microstrip Circuit Fabrication

The microstrip transmission lines used in this study are fabricated by a photo-lithographic procedure on a standard double sided dielectric substrate (Rogers Kappa 438, Rogers Corporation, Chandler, AZ, USA). A mask of the desired shape is created with the help of a laser printer on a photo- lithographic sheet. The top layer is covered with the mask in order to protect the copper that should not be removed. Excess copper is removed by the help of ferric chloride solution. A prototype obtained with this method is shown in Figure 1. The gap of the microstrip line is to be filled with graphene or biochar films.

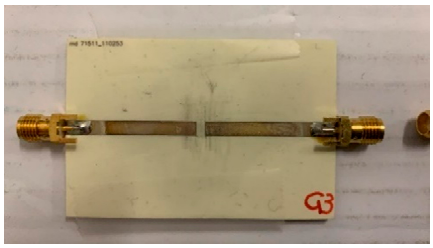

Figure 1. Prototype of the microstrip line with gap without film deposition.

The type of graphene used is in the form of nanoplatelets based on multiple graphene layers provided by Nanoinnova (Nanoinnova Technologies SL, Spain). The surface area of the nanoplatelets as provided by the manufacturer is ~45 m^2/g with a carbon content of approximately over 98.9 wt.%. The biochar used is sewage sludge biochar produced by Bioforcetech Corporation, San Francisco, CA, USA [21]. Bioforetech provide biosolids and organic waste solutions using efficient and high value processes (biodryer and pyrolysis). The biochar is produced from waste material derived from municipal waste after drying and pyrolysis. The pyrolysis process is performed in an environment lacking oxygen and thus does not involve any burning or production of flames.

The materials used as filler are biochar or graphene nanoplatelets. The film is prepared with a ratio of filler to binder of 9:1 mass ratio. The binder is a commercially available

material, polyvinylidene fluoride (PVDF). Binder provides the film with its mechanical stability and helps in adhesion. The binder is not conductive and given its small percentage in the film does not influence the electrical properties of the film to a great extent. The binder needs to be dispersed in a solvent before the addition of the filler by a stirring procedure. The solvent used for the preparation of the binder is an organic material, N-methyl-2-pyrrolidone (NMP), which facilitates the dispersion of the binder and the filler without any thermal treatment. The mixture of the binder (NMP and PVDF) and the filler is called slurry. The obtained slurries are mixed overnight, and doctor bladed on the gap.

The slurry is deposited in the designated spot on the microstrip line by hand, utilizing a mask of specific dimensions (4 mm diameter). The mask is made up of an adhesive material of uniform thickness of 500 micron. The mask is removed after the deposition of the film has dried under a laboratory hood at room temperature. This enables the evaporation of any residual solvent in the film. The coatings is let dry under hoof convection several days so not to alter the continuity between to copper branches over the dielectric substrate.

Morphological characterization of the two fillers and of the films is performed by Raman and FESEM) analysis.

2.2. Raman and FESEM Analysis

The fillers and the films were analyzed using a Renishaw InVia Raman spectrometer (Renishaw plc, Wotton-under-Edge, UK) with a 514.5 nm laser excitation using a 20× objective. The average spectrum was calculated from 5 measurements acquired on different spots on each samples. Each measurement was collected using an extended scanning mode in the 500–3000 cm^{-1} range. All the spectra were normalized using a commercial software (Origin version 8.5, OriginLab Co., Northampton, MA, USA). In addition, the ratio between the heights of the D and G peaks (I(D)/I(G)) ratio were calculated using a curve fit routine provided by the Wire 3.4 Renishaw software [22,23]. For the FESEM analysis a ZEISS SUPRA ^{TM} 40 microscope was used.

2.3. Four Point Analysis

Four point probes measurements were carried out with a Frequency Response Analyser FRA32M implemented in an Autolab electrochemical workstation provided by Metrohm, Netherlands. The frequency spans from 100 Hz to 1MHz. The amplitude of the applied voltage small signal was 5 mV and frequencies were sampled 10 points per decade.

2.4. Circuit Model

The circuit is simulated with an RF/microwave circuit design tool, AWR microwave office (Cadence, version 13, Dublin, Ireland). The simulations are performed in the frequency band of 1 GHz to 5 GHz. The dimensions of the circuits produced are 40 mm × 30 mm. The length of each line section of the microstrip line is 19 mm. The width of the line is 2.9 mm. This width corresponds to a characteristic impedance of 50 Ω. The gap between the two transmission lines is 2 mm. The dielectric substrate used for the experiments is Rogers Kappa 438. The dielectric permittivity of the substrate is, ε_r = 4.38 and loss tangent is, tan δ = 0.005.

The microstrip line with film is composed of two transmission line sections with a gap between them. The gap can be modelled as a series capacitor, Cs connecting the two-line sections and a pair of parallel capacitors, Cp representing the capacitance between the microstrip line and the ground plane as shown in Figure 2. As described in detail in [24,25] the series and parallel capacitors of a microstrip line with gap are given by:

$$C_p = 0.5C_e \quad (1)$$

$$C_s = \frac{C_o - C_p}{2} \quad (2)$$

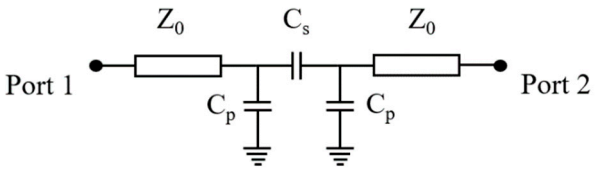

Figure 2. Circuit model representation of the microstrip line with a gap without film deposition.

A curve-fitted expression for the gap capacitance is derived in [24,25] as:

$$\frac{C_o(9.6)}{w} = \left(\frac{s}{w}\right)^{m_o} \exp(k_o)\ \text{pF/m} \tag{3}$$

$$\frac{C_e(9.6)}{w} = \left(\frac{s}{w}\right)^{m_e} \exp(k_e)\ \text{pF/m} \tag{4}$$

These expressions hold true for a dielectric material with $\varepsilon_r = 9.6$ and $0.5 < w/h < 2$. For a material with different dielectric properties this can be adjusted as:

$$\mathrm{C_o}(e_r) = \mathrm{C_o}(9.6)\left(\frac{e_r}{9.6}\right)^{0.8} \tag{5}$$

$$\mathrm{C_e}(e_r) = \mathrm{C_e}(9.6)\left(\frac{e_r}{9.6}\right)^{0.9} \tag{6}$$

To evaluate m_o, k_o and m_e, k_e for s/w ranging from 0.3 to 1 the following relations hold:

$$m_o = \frac{w}{h}\left\{0.619\ log\left(\frac{w}{h}\right) - 0.3853\right\} \tag{7}$$

$$k_o = 4.26 - 1.453\ log\left(\frac{w}{h}\right) \tag{8}$$

$$m_e = \left[1.565/(w/h)^{0.16}\right] - 1 \tag{9}$$

$$k_e = 1.97 - \frac{0.03}{w/h} \tag{10}$$

The model of the microstrip line with gap can be used in the modelling of the microstrip with films. In this case the values of the series and parallel capacitor modelled for a microstrip line without film are retained. The material deposited in the gap is represented by an impedance value as shown in Figure 3. The impedance values of the films, $Z_f = R_f + jX_f$, are obtained by tuning them to provide simulated values of scattering parameters that are comparable to the measured values.

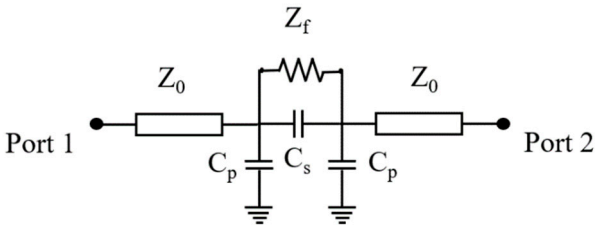

Figure 3. Circuit model representation of the microstrip line with gap including film.

2.5. Scattering Parameter Measurements

Scattering parameters measurements of the microstrip line are performed by the help of a vector network analyzer, VNA (P9371A by Keysight, Santa Rosa, CA, USA). The frequency band of the VNA is 300 kHz to 6.5 GHz. The measurements were performed in the frequency band 1–5 GHz (see Figure 4). Before each set of measurements, the VNA is calibrated at the ends of the coaxial cables with an electronic calibration kit (N7551A dc to

6.5 GHz, Keysight, Santa Rosa, CA, USA). This procedure removes systematic errors (delay on the cables, transitions, etc.).

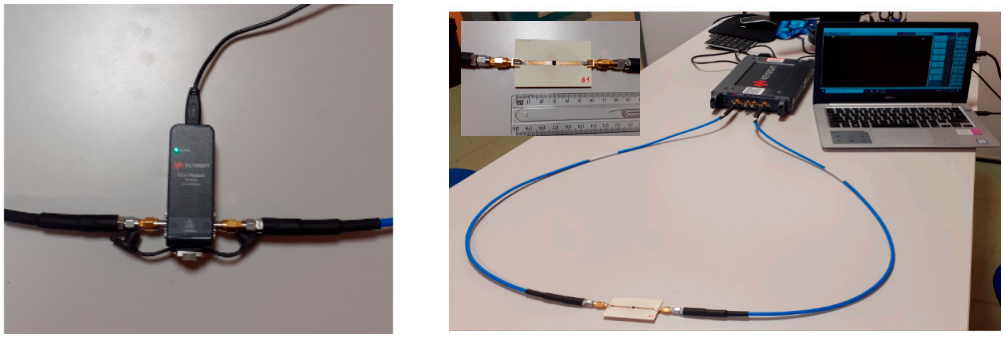

(**a**) (**b**)

Figure 4. Scattering parameters measurements: (**a**) measurement setup and microstrip line with film in the inset; (**b**) electronic calibration kit.

3. Results

3.1. Raman Characterization of Graphene and Biochar Filler and Films

The fillers (graphene nanoplatelets and biochar) and the films were characterized by Raman spectroscopy, in order to check their chemical/structural features (e.g., the presence of aromatic C) and disclose any possible damage of the carbon structure after the deposition. Figure 5 shows the obtained average spectra for both the graphene nanoplatelets (black curves) and biochar (red curves), before (Figure 5a,c) and after the deposition process (Figure 4b,d). It can be noticed that no substantial differences can be seen, meaning that the deposition process did not affect the substrates overall composition and structure. The graphene nanoplatelets spectrum (Figure 5a,b) shows defined vibrational features that are typical of graphene and graphene-like material: two close bands located at ~1350 cm^{-1} and ~1570 cm^{-1}, arising respectively from the breathing mode of the graphene ring (D peak) and from the in-plane stretching of the sp^2 carbon (G peak), and a third band at ~2690 cm^{-1} (2D peak), that is an overtone of the D band [26,27]. The intensity of the G peak, which is roughly two times higher than the 2D peak, suggests a multi-layer structure of the graphene nanoplatelets [27], whereas the presence of the D band indicates the presence of small amounts of defects, in the structure itself [28,29]. Similarly, the spectrum related to biochar (Figure 4a,d) also show vibrational features of carbonaceous materials that are coherent with the ones reported in literature [29]. It's clearly noticeable that the absence of the 2D band, as well as the broadening of the D and G bands, is due to the more disordered structure of the biochar samples compared with graphene [26,28]. As expected, the D peak appears to be more intense. Such characteristics are well highlighted by the I(D)/I(G) ratio that increase from 0.15, for the graphene, up to 1.3 of the biochar. All of these features correspond to a disordered graphitic lattice (e.g., graphene layer edges), or amorphous (partially hydrogenated) carbon, indicating the presence of small aromatic clusters [30].

3.2. FESEM Characterization of Graphene and Biochar Filler and Films

The FESEM images of the graphene nanoplatelets used as fillers in the film can be seen in Figure 6. The graphene nanoplatelets (see Figure 6a) shows that they are flaky and two dimensional. Seen with a higher magnification (see Figure 6b), They exhibit transparency, which shows that they are thin and hence composed of a few graphene layers [31]. The FESEM analysis of biochar used as filler in the films is shown in Figure 7. It can be seen that they are composed of agglomerates of carbonaceous materials with dimensions of less than 5um. It is due to their small dimensions that they are easy to disperse when mixed in a binder [32].

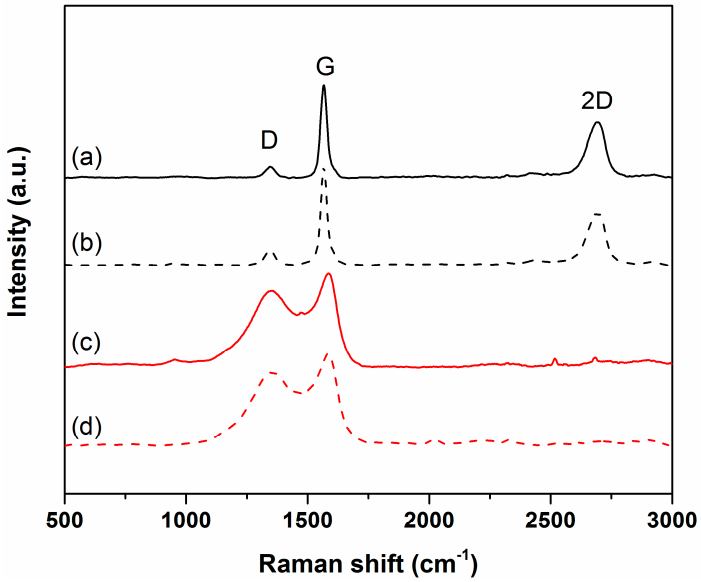

Figure 5. Raman average spectra of the fillers and films: (**a**) graphene filler (solid black line); (**b**) graphene film (dash black line); (**c**) biochar filler (solid red line); (**d**) biochar film (dash red line).

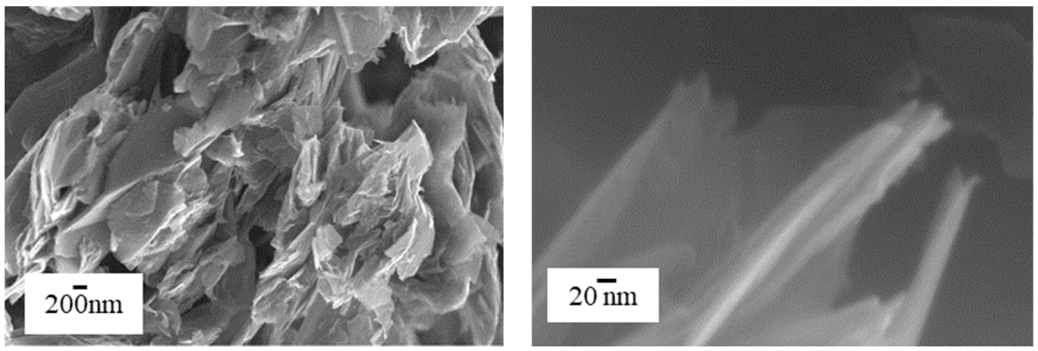

(**a**) (**b**)

Figure 6. FESEM images of commercial graphene nanoplatelets: (**a**) agglomerate of graphene flakes with magnification of 200 nm. (**b**) individual flake with magnification of 20 nm.

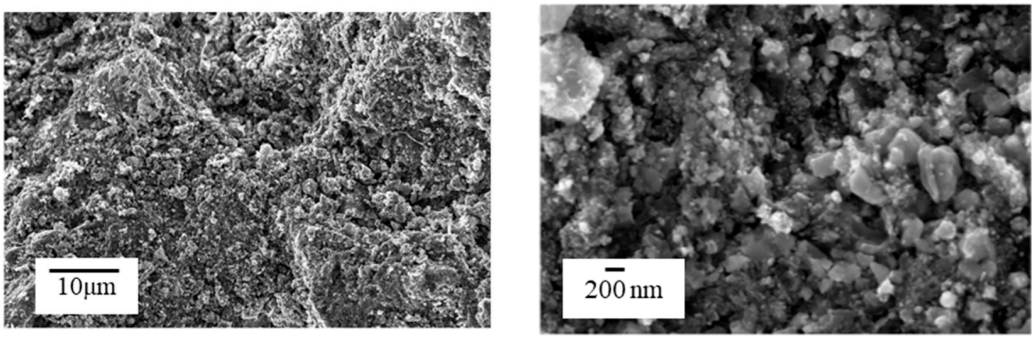

(**a**) (**b**)

Figure 7. FESEM image of the biochar filler: (**a**) overview at magnification of 10 m; (**b**) magnification of 200 nm showing the granular aspect of biochar.

In Figures 8 and 9 the FESEM images of biochar film and graphene film are reported respectively. In the case of biochar small agglomerates of the biochar is visible and seems to be well dispersed. In the graphene films, it can be seen that the nanoplatelets are well dispersed. The individual nanoplatelets are still distinguishable in the films.

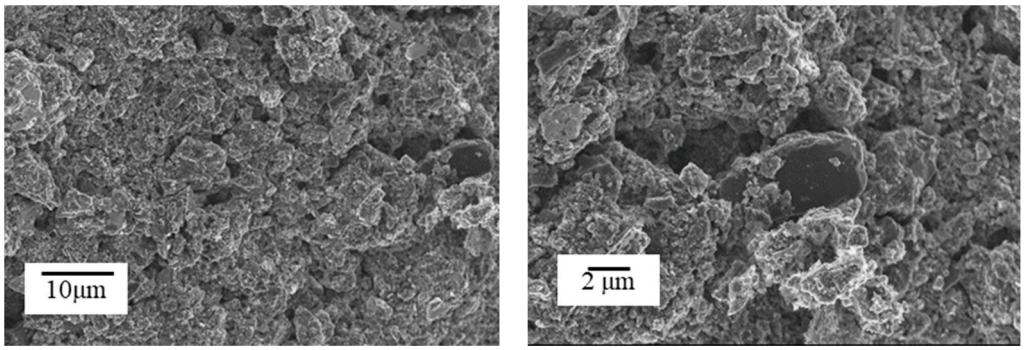

(a) (b)

Figure 8. FESEM images of biochar films: (**a**) overview of biochar film at magnification of 10 m; (**b**) magnified at 2 m, biochar film still retains granular aspect.

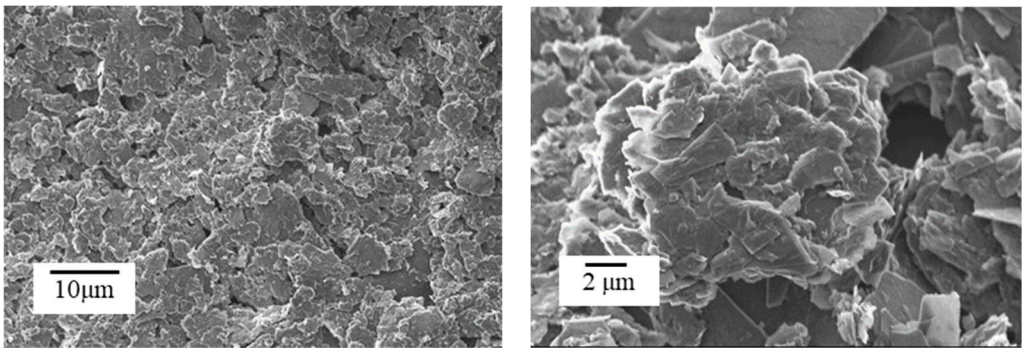

(a) (b)

Figure 9. FESEM images of graphene films: (**a**) overview of graphene film at magnification of 10 m; (**b**) magnified at 2 m, flakes embedded in graphene film can be seen.

3.3. Electrical Characterization

The four point probes measurements were carried out on the samples with graphene or biochar films. Nyquist plots have a different scale because of the different material properties. Indeed, graphene samples demonstrated a quite low resistive behaviour and, moreover, a constant response throughout the observed frequency range as can be observed from Figure 10. A charge transfer phenomenon between irregular particles is shown in biochar [33]. The broadened and irregular semi-circle shown in the Nyquist plot of Figure 11 suggests the presence of at least two time constants of this parasitic phenomenon that is responsible for high values of resistances. The overall resistivity of the biochar is not believed to be changing in the frequency range. Any direct confrontation of the results on the same plot chart would be of poor readability because of the difference in decades so this is the reason why two chart type were selected to represent the impedance measurements.

Note that the approximate aspect ratio of the deposition is 0.5. In order to obtain values independent from the geometry of the deposition, the value of resistance and reactance can be converted in the corresponding sheet resistance and reactance values by Rs (Ω/square) = 2R(Ω).

The microstrip line with gap has been modelled by the help lumped capacitors as discussed in Section 2.3. The values of series and parallel capacitances obtained from the Equations (1)–(10) are: Cp = 0.0043 pF, Cs = 0.019 pF. These values are used in the circuit model simulations to acquire two port scattering parameters as shown in Figure 2. The scattering parameters of the microstrip line without any film depositions are measured with a VNA. The simulated and measured scattering parameters are reported in Figure 12. It can be seen that both the amplitude and phase of the reflection and transmission for the simulated and measured scattering parameters are in good agreement.

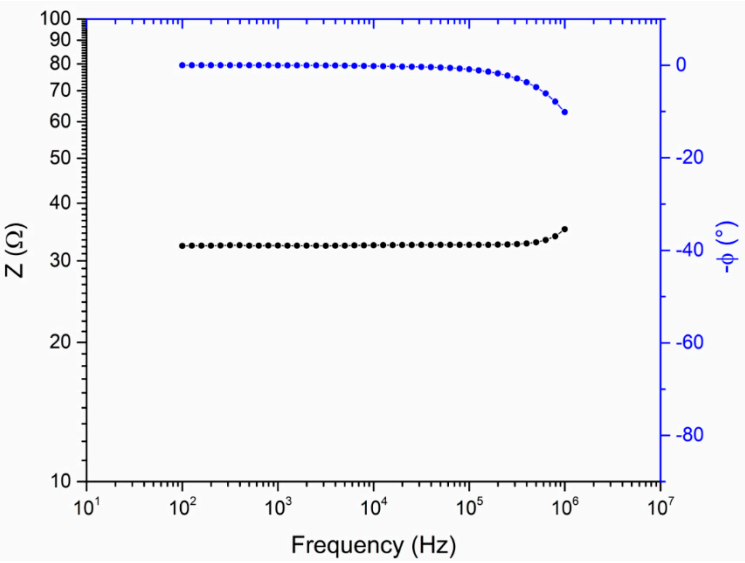

Figure 10. Bode Plot of the graphene sample. Black curve represents the amplitude of the impedance (vertical axis on the left). Blue curve represents the phase of the impedance (vertical axis on the right). At high frequencies some distortions due to the experimental setup.

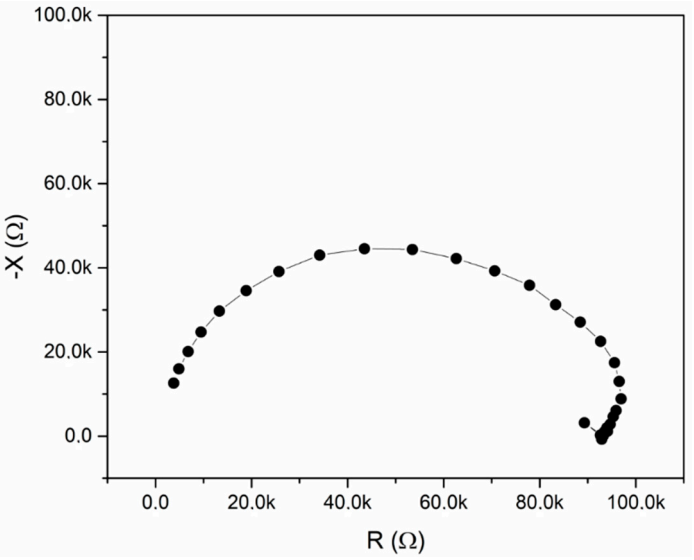

Figure 11. Nyquist plot of the Biochar sample in which charge transfer phenomenons are evident because of the broadened semi-circle.

In a similar manner, measurements of the scattering parameters of the microstrip lines with biochar and graphene films are performed. In the case of microstrip lines with film, the film is added as a lumped impedance.

Amplitude and phase of the simulated scattering parameters can be varied by varying the impedance of the films. A fitting procedure is adopted for the acquisition of simulated values of scattering parameters that are comparable to the measured values. For the biochar films the values are R_f = 10.36 KΩ and X_f = 1.82 KΩ, whereas for the graphene films R_f = 33 Ω and X_f = −12 Ω The simulated and measured values of the reflection and transmission scattering of the microstrip line with biochar film are shown in Figure 13. Being less conductive, the transmission scattering of the film with biochar is less than −30 dB. The simulated and measured scattering parameters of the microstrip line with graphene film are shown in Figure 14. The conductivity of graphene is high and results in a transmission scattering of almost −3 dB.

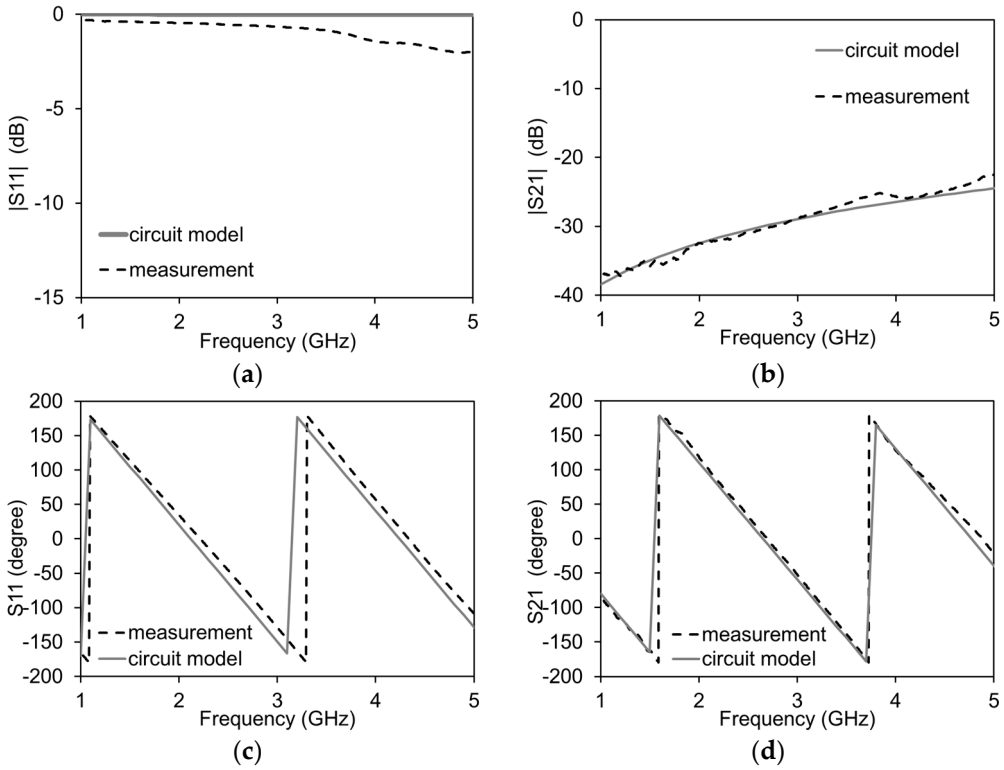

Figure 12. Simulated (solid lines) and measured (dashed lines) scattering parameters of gap: (**a**) amplitude of reflection coefficient (dB); (**b**) amplitude of transmission coefficient (dB); (**c**) phase of the reflection coefficient (deg); (**d**) phase of the transmission coefficient (deg).

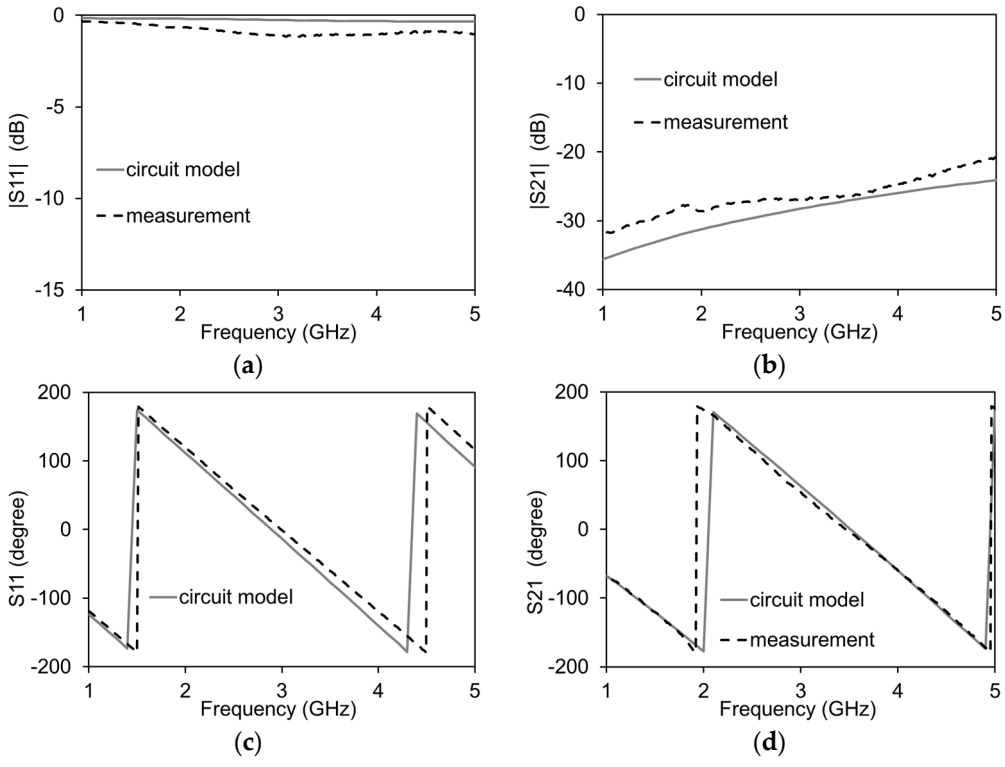

Figure 13. Simulated (solid lines) and measured (dashed lines) scattering parameters of biochar film: (**a**) amplitude of reflection coefficient (dB); (**b**) amplitude of transmission coefficient (dB); (**c**) phase of the reflection coefficient (deg); (**d**) phase of the transmission coefficient (deg).

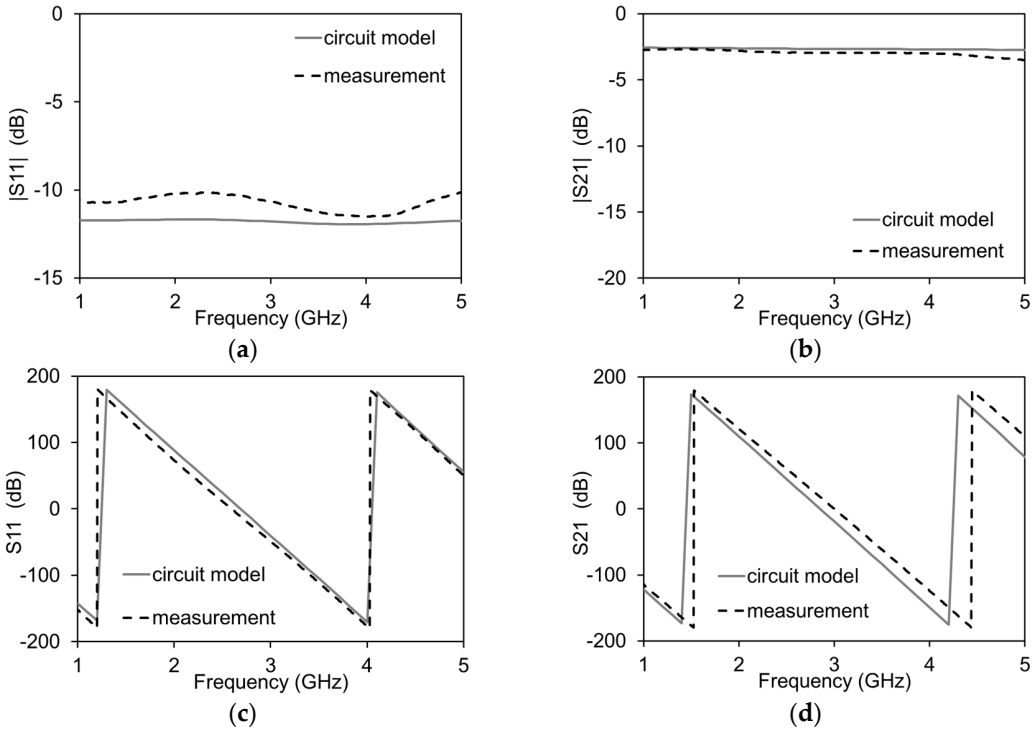

Figure 14. Simulated (solid lines) and measured (dashed lines) scattering parameters of graphene films: (**a**) amplitude of reflection coefficient (dB); (**b**) amplitude of transmission coefficient (dB); (**c**) phase of the reflection coefficient (deg); (**d**) phase of the transmission coefficient (deg).

4. Discussion

Novel materials are usually characterized at microwave frequencies by different methods including open- ended coaxial probe, parallel plate, coaxial or waveguide transmission lines, resonant cavity methods, waveguide methods and free-space methods [34,35]. These methods are generally suitable for bulk materials or materials covering large dimensions. Furthermore, the material under test should fit in a precise enclosure imposing stringent shape requirements. These methods are not suitable for the characterization of films. The possibility to deposit films under test on a gap in a microstrip line and modeling the film as lumped elements can be an additional tool for the characterization of films. Moreover, the deposition of films in a gap on a microstrip line is easier and does not require a precise shape. The dimensions of the material deposited can be considered at a later stage and values represented as a function of area.

The morphological characterization performed on the filler and the film shows a similar behavior since a major portion of the film comprises of the filler. Biochar exhibits a more disordered structure as compared to graphene which can be seen in the absence of the 2D band and the broadening of the D and G bands in Raman spectroscopy results. Furthermore, it can be seen that the I(D)/I(G) ratio is higher in biochar than in graphene which shows a disordered graphitic lattice in graphene or amorphous carbon in biochar. From the FESEM analysis of the graphene and biochar filler and films, it can be seen that they are well dispersed in the binder. The graphene nanoplatelets are distinguishable in the films. The biochar agglomerates are small and aids in the dispersion in the composite film. The FESEM images of the biochar films and powders show the presence of rounded particles while graphene shows the presence of flakes. Both being carbonaceous, the conductivity of the individual particles of the two materials could not be very different. In the case of biochar, the particle-particle contact is not optimal causing a resistive behavior. On the contrary, graphene film contains flake-like particles in which there is more particle-particle contact. This increases the transport properties making graphene fillers more conductive.

The four-point probe measurements performed in the frequency range 100 KHz–1 MHz confirms this behavior since graphene show an average constant modulus in the impedance lower than the biochar. Moreover, the scarce transport properties of biochar are further confirmed by the presence of capacitive phenomenon as observed from the Nyquist plot [33].

The analysis of films in the form of lumped elements facilitates their deployment in circuits and systems. The modelling of the microstrip line gap with series and parallel capacitors provides comparable values of scattering parameters. It permits to characterize the film as an impedance with a real part (resistance) and imaginary part (reactance). A variation of the resistance drastically varies the amplitude of the transmitted signal with a small impact on its phase. The variation of reactance drastically varies the phase of the transmitted signal. The comparable values of both the amplitude and phase of the transmitted and reflected signal shows that the values of resistance and reactance are accurate. Once the lumped element values of the film are known in a given situation they are useful in designing circuits and systems [36–39]. If the films are to be deployed in sensing applications these can be used to signal the indication of a particular situation (the presence of a specific gas, a given pressure, a value of humidity, electromagnetic power or the like).

5. Conclusions

The morphological and electrical properties of graphene and biochar in the form of fillers and films are investigated. From the Raman and FESEM it can be deduced that graphene films consist of interconnecting multiple layered graphene nanoplatelets forming a network. This makes them more conductive than biochar films which from the morphological characterization seems disordered and granulated. Resistance and reactance values derived from DC, low frequency and high frequency lumped models also show that graphene has low resistance and reactance values while biochar has high resistance and reactance values. These considerations make graphene films suitable for applications where higher conductivity values are required like tunable electronic devices, sensing and detection while biochar being low cost is more suitable for applications where higher volumes are required e.g., polymers and cements etc.

Author Contributions: Conceptualization, P.S., M.Y. and P.Z.; methodology P.S., M.Y., F.F., G.P.; software, M.Y.; Raman analysis, N.P.; writing—original draft preparation, P.S., M.Y., P.Z., N.P.; writing—review and editing, P.S. and M.Y.; funding acquisition, P.S. All authors have read and agreed to the published version of the manuscript.

Funding: This research was funded by Proof of Concept 2018 program, Vertis SGR, Milan, Italy.

Acknowledgments: The authors would like to acknowledge Matteo Longo of Bioforcetech Corporation for supplying the biochar and Salvatore Guastella and Mauro Raimondo for FESEM.

Conflicts of Interest: The authors declare no conflict of interest.

References

1. Castro Neto, A.H.; Guinea, F.; Peres, N.M.R.; Novoselov, K.S.; Geim, A.K. The electronic properties of graphene. *Rev. Mod. Phys.* **2009**, *81*, 109. [CrossRef]
2. Thomas, D.-G.; Kavak, E.; Hashemi, N.; Montazami, R.; Hashemi, N.N. Synthesis of Graphene Nanosheets through Spontaneous Sodiation Process. *C J. Carbon Res.* **2018**, *4*, 42. [CrossRef]
3. Khurram, A.A.; Rakha, S.A.; Zhou, P.; Shafi, M.; Munir, A. Correlation of electrical conductivity, dielectric properties, microwave absorption, and matrix properties of composites filled with graphene nanoplatelets and carbon nanotubes. *J. Appl. Phys.* **2015**, *118*, 044105. [CrossRef]
4. Bellucci, S.; Maffucci, A.; Maksimenko, S.; Micciulla, F.; Migliore, M.D.; Paddubskaya, A.; Pinchera, D.; Schettino, F. Electri-cal Permittivity and Conductivity of a Graphene Nanoplatelet Contact in the Microwave Range. *Materials* **2018**, *11*, 2519. [CrossRef] [PubMed]
5. Zinenko, T.L.; Matsushima, A.; Nosich, A.I. Surface-plasmon, grating-mode and slab-mode resonances in THz wave scat-tering by a graphene strip grating embedded into a dielectric slab. *IEEE J. Sel. Topics Quant. Electron.* **2017**, *23*, 4601809. [CrossRef]

6. Xia, J.; Chen, F.; Li, J.; Tao, N. Measurement of the quantum capacitance of graphene. *Nat. Nanotechnol.* **2009**, *4*, 505–509. [CrossRef] [PubMed]
7. Enzheng, S.; Hongbian, L.; Long, Y.; Junfeng, H.; Yuanchang, L.; Li, L.; Anyuan, C.; Ying, F. Carbon Nanotube Network Em-broidered Graphene Films for Monolithic All-Carbon Electronics. *Adv. Mater.* **2015**, *27*, 682–688.
8. Su, W.; Xu, J.; Ding, X. An Electrochemical pH Sensor Based on the Amino-Functionalized Graphene and Polyaniline Com-posite Film. *IEEE Trans. Nanobiosci.* **2016**, *15*, 812–819. [CrossRef]
9. Itapu, B.M.; Jayatissa, A.H. A Review in Graphene/Polymer Composites. *Chem. Sci. Int. J.* **2018**, *23*, 1–16. [CrossRef]
10. Ferrari, A.C.; Meyer, J.C.; Scardaci, V.; Casiraghi, C.; Lazzeri, M.; Mauri, F.; Piscanec, S.; Jiang, D.; Novoselov, K.S.; Roth, S.; et al. Raman Spectrum of Graphene and Graphene Layers. *Phys. Rev. Lett.* **2006**, *97*, 187401. [CrossRef]
11. González, R.; González, J.; Rosas, J.G.; Smith, R.; Gómez, X. Biochar and Energy Production: Valorizing Swine Manure through Coupling Co-Digestion and Pyrolysis. *C J. Carbon Res.* **2020**, *6*, 43. [CrossRef]
12. Ohra-Aho, T.; Lindfors, C.; Lehtonen, J.; Tamminen, T.; Siipola, V. Activated Carbons from Fast Pyrolysis Biochar as Novel Catalysts for the Post-Treatment of Pyrolysis Vapors, Studied by Analytical Pyrolysis. *C J. Carbon Res.* **2020**, *6*, 65. [CrossRef]
13. Bedia, J.; Peñas-Garzón, M.; Gómez-Avilés, A.; Rodriguez, J.J.; Belver, C. A Review on the Synthesis and Characterization of Biomass-Derived Carbons for Adsorption of Emerging Contaminants from Water. *C J. Carbon Res.* **2018**, *4*, 63. [CrossRef]
14. Tolkou, A.K.; Zouboulis, A.I. Graphene Oxide/Fe-Based Composite Pre-Polymerized Coagulants: Synthesis, Characterization, and Potential Application in Water Treatment. *C J. Carbon Res.* **2020**, *6*, 44. [CrossRef]
15. Richards, K.R.; Stokes, C. A Review of Forest Carbon Sequestration Cost Studies: A Dozen Years of Research. *Clim. Chang.* **2004**, *63*, 1–48. [CrossRef]
16. Das, O.; Sarmah, A.K.; Bhattacharyya, D. Biocomposites from waste derived biochars: Mechanical, thermal, chemical, and morphological properties. *Waste Manag.* **2016**, *49*, 560–570. [CrossRef]
17. Giorcelli, M.; Savi, P.; Khan, A.; Tagliaferro, A. Analysis of biochar with different pyrolysis temperatures used as filler in epoxy resin composites. *Biomass Bioenergy* **2019**, *122*, 466–471. [CrossRef]
18. Andersson, M.; Habibpour, O.; Vukusic, J.; Stake, J. 10 dB small-signal graphene FET amplifier. *Electron. Lett.* **2012**, *48*, 861. [CrossRef]
19. Savi, P.; Naishadham, K.; Quaranta, S.; Giorcelli, M.; Bayat, A. Microwave characterization of graphene films for sensor applications. In Proceedings of the 2017 IEEE International Instrumentation and Measurement Technology Conference (I2MTC), Turin, Italy, 22–25 May 2017; pp. 1–5. [CrossRef]
20. Quaranta, S.; Miscuglio, M.; Bayat, A.; Savi, P. Morphological and Radio Frequency Characterization of Graphene Composite Films. *C J. Carbon Res.* **2018**, *4*, 32. [CrossRef]
21. Available online: www.bioforcetech.com (accessed on 25 March 2021).
22. Ferrari, A.C.; Basko, D.M. Raman spectroscopy as a versatile tool for studying the properties of graphene. *Nat. Nanotechnol.* **2013**, *8*, 235–246. [CrossRef]
23. Bokobza, L.; Bruneel, J.-L.; Couzi, M. Raman Spectra of Carbon-Based Materials (from Graphite to Carbon Black) and of Some Silicone Composites. *C J. Carbon Res.* **2015**, *1*, 77–94. [CrossRef]
24. Garg, L.; Bahl, I.J. Microstrip discontinuities. *Int. J. Electron.* **1978**, *45*, 81–87. [CrossRef]
25. Edwards, T.C.; Steer, M.B. Discontinuities in microstrip and stripline. In *Foundations of Interconnect and Microstrip Design*, 1st ed.; Wiley & Sons Ltd.: Hoboken, NJ, USA, 2000; pp. 225–268.
26. Björkman, C.-I.Å. Thermische Klärschlammbehandlung. *Aquat. Sci.* **1969**, *31*, 632–645. [CrossRef]
27. Roppolo, I.; Chiappone, A.; Bejtka, K.; Celasco, E.; Chiodoni, A.; Giorgis, F.; Sangermano, M.; Porro, S. A powerful tool for graphene functionalization: Benzophenone mediated UV-grafting. *Carbon* **2014**, *77*, 226–235. [CrossRef]
28. Wu, J.-B.; Lin, M.-L.; Cong, X.; Liu, H.-N.; Tan, P.-H. Raman spectroscopy of graphene-based materials and its applications in related devices. *Chem. Soc. Rev.* **2018**, *47*, 1822–1873. [CrossRef]
29. Yang, D.; Velamakanni, A.; Bozoklu, G.; Park, S.; Stoller, M.; Piner, R.D.; Stankovich, S.; Jung, I.; Field, D.A.; Ventrice, C.A.; et al. Chemical analysis of graphene oxide films after heat and chemical treatments by X-ray photoelectron and Micro-Raman spectroscopy. *Carbon* **2009**, *47*, 145–152. [CrossRef]
30. Fuertes, A.B.; Arbestain, M.C.; Sevilla, M.; Maciá-Agulló, J.A.; Fiol, S.; López, R.; Smernik, R.J.; Aitkenhead, W.P.; Arce, F.; Macias, F. Chemical and structural properties of carbonaceous products obtained by pyrolysis and hydrothermal carbonisa-tion of corn stover. *Aust. J. Soil Res.* **2009**, *48*, 618–626. [CrossRef]
31. Yasir, M.; Savi, P. Dynamically Tunable Phase Shifter with Commercial Graphene Nanoplatelets. *Micromachines* **2020**, *11*, 600. [CrossRef]
32. Yasir, M.; Savi, P. Commercial graphene nanoplatelets-based tunable attenuator. *Electron. Lett.* **2020**, *56*, 184–187. [CrossRef]
33. Dsoke, S.; Tian, X.; Täubert, C.; Schlüter, S.; Wohlfahrt-Mehrens, M. Strategies to reduce the resistance sources on Electro-chemical Double Layer Capacitor electrodes. *J. Power Sources* **2013**, *238*, 422–429. [CrossRef]
34. Krupka, J. Frequency domain complex permittivity measurements at microwave frequencies. *Meas. Sci. Technol.* **2006**, *17*, R55–R70. [CrossRef]
35. Ghodgaonkar, D.; Varadan, V. Free-space measurement of complex permittivity and complex permeability of magnetic materials at microwave frequencies. *IEEE Trans. Instrum. Meas.* **1990**, *39*, 387–394. [CrossRef]
36. Li, B.; Zhong, W.-H. Review on polymer/graphite nanoplatelet nanocomposites. *J. Mater. Sci.* **2011**, *46*, 5595–5614. [CrossRef]

37. Byrne, M.T.; Guin'Ko, Y.K. Recent advances in research on carbon nanotube – polymer composites. *Adv. Mater.* **2012**, *22*, 1672–1688. [CrossRef] [PubMed]
38. Giambra, M.; Benfante, A.; Zeiss, L.; Pernice, R.; Miseikis, V.; Pernice, W.; Jang, M.; Ahn, J.; Cino, A.; Stivala, S.; et al. Layout influence on microwave performance of graphene field effect transistors. *Electron. Lett.* **2018**, *54*, 984–986. [CrossRef]
39. Yasir, M.; Aldrigo, M.; Dragoman, M.; Dinescu, A.; Bozzi, M.; Iordanescu, S.; Vasilache, D. Integration of Antenna Array and Self-Switching Graphene Diode for Detection at 28 GHz. *IEEE Electron. Device Lett.* **2019**, *40*, 628–631. [CrossRef]